# Lateral Diffusion Measurement at High Spatial Resolution by Scanning Microphotolysis in a Confocal Microscope

Ulrich Kubitscheck, Peter Wedekind, and Reiner Peters
Institut für Medizinische Physik und Biophysik, Westfälische Wilhelms-Universität Münster, 48149 Münster, Germany

ABSTRACT Fluorescence photobleaching methods have been widely used to study diffusion processes in the plasma membrane of single living cells and other membrane systems. Here we describe the application of a new photobleaching technique, scanning microphotolysis. Employing a recently developed extension module to a commercial confocal microscope, an intensive laser beam was switched on and off during scanning according to a user definable image mask. Thereby the location, geometry, and number of photolysed spots could be chosen arbitrarily, their size ranging from tens of micrometers down to the diffraction limit. Therewith we bleached circular areas on the surface of single living 3T3 cells labeled with the fluorescent lipid analog NBD-HPC. Subsequently, the fluorescence recovery process was observed using the attenuated laser beam for excitation. This yielded image stacks representing snapshots of the spatial distribution of fluorescent molecules. From these we computed the radial distribution functions of the photobleached dye molecules. The variance of these distributions is linearly related to the diffusion constant, time, and the mobile fraction of the diffusing species. Furthermore, we compared directly the theoretically expected and measured distribution functions, and could thus determine the diffusion coefficient from each single image. The results of these two new evaluation methods ($D = 0.3 \pm 0.1\ \mu m^2/s$) agreed well with the outcome of conventional fluorescence recovery measurements. We show that by scanning microphotolysis information on dynamical processes such as diffusion of lipids or proteins can be acquired at the superior spatial resolution of a confocal laser scanning microscope.

## INTRODUCTION

The fluorescence photobleaching method has become an important tool in investigating the transport of biological molecules within and across cellular membranes (Thomas and Webb, 1990; Petersen et al., 1986; Peters and Scholz, 1991). The technique is generally based on photolysis of fluorescently labeled components within a small spot. The analysis of the dissipation of the gradient in the distribution of fluorescent dye molecules yields information on the mobility characteristics of the labeled species such as the diffusion coefficient and size of the mobile fraction (Peters et al., 1974; Axelrod et al., 1976; Jacobson et al., 1976; Edidin et al., 1976).

So far, fluorescence photobleaching is a single-cell technique, and one can measure diffusion on multiple regions of the same cell only in subsequent experiments. In these spot measurements, the signal obtained is an integral over a defined area in the observation field. As a result, all spatial and directional information is averaged out and lost.

However, recent experimental and numerical studies indicate that the dynamics of biological membranes is more complex than imagined in the early days of photobleaching techniques (Saxton, 1993; Edidin, 1992; Ishihara and Jacobson, 1993). These findings point to the requirement for advanced experimental techniques that allow the examination of the dynamic processes at high spatial resolution. Single-particle tracking is a new experimental method to examine the dynamics on cell surfaces at the molecular level (Kusumi et al., 1993; Jacobson et al., 1994; Webb, 1994). Another approach is the extension of photobleaching techniques to spatially resolved measurements of distributions of molecules on cell surfaces. This can be achieved by using imaging systems for monitoring the dynamic process after photobleaching, thus obtaining spatial information about membrane transport processes on a submicrometer length scale (Kapitza et al., 1985; Tsay and Jacobson, 1991; Cardullo et al., 1991; Jain et al., 1990). Spatially resolved photobleaching techniques can detect anisotropic diffusion, or the rates of diffusional exchange between morphologically distinct regions of a cell (Tsay and Jacobson, 1991). Another obvious advantage of two-dimensional observation of the dynamic process is that drift of the photobleached area is immediately noticed and can be dealt with separately.

Employing a confocal laser scanning microscope (CLSM) adds even more advantageous features to high resolution photobleaching measurements. (i) True three-dimensional imaging facilities can be used for inspecting and selecting the site for the bleach experiment. (ii) Because of the high depth resolution of confocal imaging provided by using very small illumination and detection pinholes, background fluorescence is much more efficiently rejected than in the conventional photobleaching setup, in which much larger pinholes are used, or in systems without pinholes employing CCD cameras. (iii) By the high depth resolution, contributions of internalized dye molecules are largely suppressed, and the process of internalization of fluorescent markers can even be monitored. (iv) Photobleaching measurements in thick and

*Received for publication 23 March 1994 and in final form 31 May 1994.*
Address reprint requests to Dr. Reiner Peters, Institut fur Medizinische Physik und Biophysik, Westfalische, Wilhelms-Universitat, Munster, 48149 Munster, Germany. Tel.: 251-836933; Fax: 251-835121; E-mail: petersr@asterix.uni-muenster.de.

0006-3495/94/09/948/09 $2.00

scattering samples are feasible because of the absence of out-of-focus contributions (Blonk et al., 1993).

The advantages of confocal scanning for measurements of lateral mobility in membranes were first exploited by Koppel (1979), who incorporated a galvanometric optical scanner into the excitation pathway of a photobleaching instrument. By these means, a focused laser beam could be rapidly scanned back and forth over the object along a linear pathway. The fluorescence of the scanned pathway could be imaged semi-confocally (i.e., via a slit) and analyzed before and after photobleaching. Later on, Cooper et al. (1990), studying the dynamics of cytoskeletal fibers, employed a commercial nonmodified CLSM to image and bleach linear pathways in cells. Scholz et al. (1988) equipped a confocal laser scanning microscope (CLSM) with a second, more powerful laser to bleach small circular areas while using the internal laser to generate confocal images before and after bleaching. Recently, Blonk et al. (1993) described a photobleaching technique in which a CLSM was also operated in the mode in which only one line, instead of a complete frame, was scanned. Photobleaching was achieved by halting the scanning mirrors for defined times before resuming line scanning.

Here we apply a new photobleaching technique, scanning microphotolysis, Scamp (Kubitscheck et al., 1994; Wedekind et al., 1994), that does not only take advantage of the superior spatial resolution but also uses the scanning mode operation of a CLSM for photobleaching. Employing a soft- and hardware extension module to a commercial CLSM, the laser beam can be switched on and off during the scanning process of the CLSM in accordance with a user-definable image mask. This leaves complete freedom in the choice of the size, location, geometry, and even number of the bleached spots. After creating the photolysis pattern in the sample, we monitor the recovery process by a series of images attained using a low intensity laser beam for excitation.

Scamp experiments yield image stacks as raw data documenting the fluorescence recovery process at the resolution of a confocal microscope. Each image represents a snapshot of the spatial distribution of the nonphotolysed molecules at a defined time point. Hence, the image stacks contain a wealth of spatial information on the observed dynamic process. We suggest two new concepts for evaluating this large amount of information in terms of lateral diffusion coefficients.

## THEORY

### Fundamentals

The analysis of diffusion measurements by photobleaching is usually based on the following considerations (Axelrod et al., 1976). Before measurements, the cellular components to be studied are labeled by fluorescent dye molecules in some direct or indirect way. The fluorescent components are supposed to be uniformly distributed in the plane of the membrane. A sufficiently strong laser pulse illuminates and bleaches the fluorophores in a small, radially symmetrical area with an intensity distribution $I(r)$, $r$ designating the distance from the center of the bleached spot. Photobleaching is assumed to be irreversible, and of first order with rate constant $K = \alpha I(r)$. After photolysis, the space- and time dependence of the concentration $c(r, t)$ of unbleached fluorophore is determined by the diffusion equation

$$\frac{\partial c(r, t)}{\partial t} = D\left[\frac{\partial^2}{\partial r^2} + \frac{1}{r}\frac{\partial}{\partial r}\right] c(r, t), \tag{1}$$

with the boundary condition $c(\infty, t) = c_0$. $D$ is the diffusion coefficient. We assume that the duration of bleaching, $T$, is negligibly small as compared with the time required for any significant transport. In this case, the fluorophore concentration profile at the beginning of the recovery phase ($t = 0$) is given by

$$c(r, 0) = c_0 e^{-\alpha I(r)T}, \tag{2}$$

where $c_0$ is the spatially constant fluorophore concentration before the experiment. In our experiments, the sample is illuminated by a beam with a uniform circular disk profile of radius $w$. The concentration of photolysed fluorophores, designated as $c^*(r, t) = c_0 - c(r, t)$, is given by (Soumpasis, 1983)

$$c^*(r, t) = c_0 w[1 - e^{-K}] \int_0^\infty e^{-Ds^2} J_0(sr) J_1(ws)\, ds. \tag{3}$$

Here, $J_n(x)$ represents the Bessel function of order $n$. The time-dependent fluorescence intensity $F(t)$ emitted from the total photolysed area being illuminated with a monitor beam, which has the same intensity profile as the bleaching beam but is attenuated by the factor $A$, is given by

$$F(t) = 2\pi \frac{q}{A} \int_0^\infty I(r) c(r, t) r\, dr, \tag{4}$$

where $q$ is the product of quantum efficiencies of light absorption, emission, and detection. It is convenient at this stage to define the fractional fluorescence $f(t)$ as

$$f(t) = \frac{F(t) - F(0)}{F(\infty) - F(0)}. \tag{5}$$

Then (Soumpasis, 1983)

$$f(t) = e^{-2\tau/t}\left[I_0\left(\frac{2\tau}{t}\right) + I_1\left(\frac{2\tau}{t}\right)\right], \tag{6}$$

with $I_n(x)$ representing modified Bessel functions of order $n$, and $\tau = w^2/4D$ the characteristic diffusion time. If only a fraction $k$ of the fluorescently labeled molecules is mobile, this is given by

$$k = \frac{F(\infty) - F(0)}{F_0 - F(0)}, \tag{7}$$

where $F_0$ denotes the fluorescence before the bleaching.

### Relation among diffusion coefficient, mobile fraction, and variance

Here we show that the convolution integral of an arbitrary initial distribution of dye molecules with the system's response to a delta function as initial distribution is a general solution of the diffusion equation, Eq. 1. We then find that the diffusion coefficient can simply be derived from the time dependence of the second central moment.

Assuming that all molecules are concentrated at the origin of the coordinate system at $t = 0$, their initial (normalized) distribution profile is equal to the product of delta functions, $\delta(x)\delta(y)$. The time development of this distribution $g_\delta(x, y, t)$is (Crank, 1975)

$$g_\delta(x, y, t) = \frac{k}{4\pi Dt} e^{-(x^2+y^2)/4Dt} + (1 - k)\delta(x)\delta(y). \quad (8)$$

We have included into this expression the parameter $k$ to account for mobile and immobile fractions within the distribution. We now consider an arbitrary, properly normalized initial distribution, $g_0(x, y)$, of a population of diffusing particles, and set the origin of our coordinate system at the mean values, $\bar{x}$ and $\bar{y}$. The time development of this distribution can be found by the convolution of $g_0(x, y)$ and $g_\delta(x, y, t)$:

$$g(x, y, t) = \frac{k}{4\pi Dt} \int\int_F g_0(\alpha, \beta)\, e^{-[(x-\alpha)^2+(y-\beta)^2]/4Dt}\, d\alpha\, d\beta + (1 - k)g_0(x, y), \quad (9)$$

where the integral includes the complete surface $F$. The sum of the two diagonal second moments, $\mu_2(t) = \langle x(t)^2 + y(t)^2\rangle$, also referred to as variance, is defined as

$$\mu_2(t) = \int\int_F (x^2 + y^2)\, g(x, y, t)\, dx\, dy. \quad (10)$$

Inserting Eq. 9 into Eq. 10, and exchanging the sequence of integration, the inner integral can be solved using some well known integral identities of the Gauss distribution function. Eventually, it can be shown that $\mu_2(t)$ is linearly related to $D$, $k$, and $t$:

$$\mu_2(t) = 4kDt + \langle x_0^2\rangle + \langle y_0^2\rangle. \quad (11)$$

It may be noted that the time dependence of the variance, $\mu_2(t)$, is independent of the initial distribution $f_0(x, y)$ and, hence, can be used to determine $D$ for arbitrary radially symmetrical initial distributions.

### Determination of diffusion coefficient and mobile fraction

The above considerations suggest three strategies for evaluating photobleaching experiments in terms of diffusion coefficients and mobile fractions.

(i) The radial distribution function of photolysed fluorophores at times $t_i$ after photobleaching is given by Eq. 3. For each time point, the radial distribution is completely determined by the radius of the bleached area, $w$, the extent of bleaching, $\alpha I(r)$, the diffusion constant, $D$, and the mobile fraction, $k$. Hence, a fit of Eq. 3 to the distribution data yields the unknown parameters.

(ii) Plotting the variance, $\mu_2(t)$, against time yields a straight line, the slope of which is equal to the product of diffusion constant and mobile fraction divided by four (eq. 11). The relaxation process must be observed until equilibrium is reached to determine the mobile fraction according to Eq. 7. Unfortunately, this method does not provide an independent way to determine $k$.

(iii) In addition, the integral fluorescence of the photobleached area can be used to derive $D$, and $k$ from Eqs. 5–7, analogous to conventional photobleaching measurements.

## MATERIALS AND METHODS

### Reagents

2-(6-(7-nitrobenz-2-oxa-1,3-diazol-4-yl)amino)hexanoyl-1-hexadecanoyl-*sn*-glycero-3-phosphocholine (NBD-$C_6$-HPC) was obtained from MOLECULAR PROBES (Eugene, OR). The lipid analog was dissolved in ethanol, aliquoted, dried under $N_2$, and stored at −20°C. Before use, the lipid analog was dissolved in phosphate buffered saline at 10 μg/ml.

### Cells and their labeling

3T3 cells were cultured in DMEM complete medium (Boehringer, Mannheim, Germany) at 37°C with 5% $CO_2$ and passaged every three days. For photobleaching studies, cells were used 24–48 h after seeding on coverslips, washed in 4 ml of DMEM without phenol red supplemented with 20 mM HEPES (Boehringer), and incubated with NBD-$C_6$-HPC (10 μg/ml) for 5 min at room temperature. After washing, the coverslips were mounted upside down on glass slides using spacers to create a little chamber containing about 30 μl of DMEM. Such samples were examined and measured for up to 60 min at room temperature ($T$ = 23 ± 2°C). Visual inspection as well as optical sections in both the $xy$ and the $xz$ plane obtained by confocal scanning showed that the lipid analog was exclusively localized in the plasma membrane during the measurements.

### Conventional photobleaching experiments

For comparison, photobleaching experiments were also performed using the conventional setup described previously (Peters and Scholz, 1991; Tschödrich-Rotter, 1994). In short, labeled samples were placed on the stage of an inverted epi-fluorescence microscope. Employing the 488-nm line of an argon laser (model 2025, Spectra Physics, Darmstadt, Germany) a circular area (radius 2.1 μm) of the sample was uniformly illuminated. Fluorescence originating from the illuminated area was measured using a single-photon counting system. For bleaching, the beam power was increased by a factor of $10^4$. A microcomputer was used for data acquisition and analysis.

### Scanning microphotolysis

We have recently developed (Kubitscheck et al., 1994; Wedekind et al., 1994) a new photobleaching technique, referred to as scanning microphotolysis (Scamp). A CLSM (Leica, Heidelberg, Germany) was complemented with a powerful argon laser (model 2025, Spectra Physics) and a novel device, the Scamper (Fig. 1). The laser was tuned to 488 nm with an output power of 1 W. In the Scamper, the laser beam passed a filter changer that contained three neutral density filters. The filters with transmission coefficients of 0.5, 0.1, and 0.03, respectively, could be motorically inserted into the laser beam in any combination yielding relative beam powers between 0.0015 and 1.0. The laser beam then entered an acousto-optical modulator (AOM, model 304, Coherent, Rödermark/Oberkochen, Germany) that

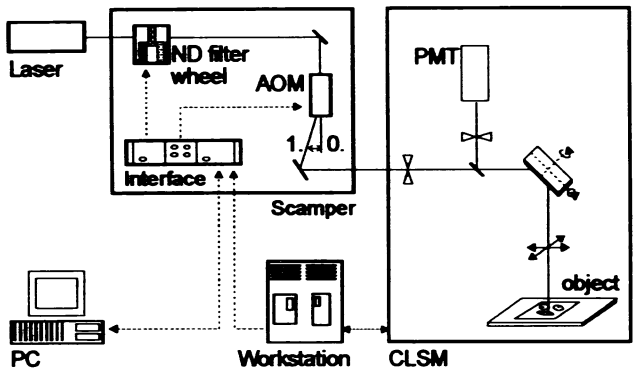


FIGURE 1 Scanning microphotolysis (Scamp), a new method combining photobleaching with laser beam scanning and confocal imaging. As indicated in the scheme, a confocal laser scanning microscope (CLSM) was complemented with powerful argon laser and a novel device, referred to as "Scamper." The scamper essentially consisted of two components in series, a filter changer that could attenuate the laser beam by a factor of approximately 1,000, and an acousto-optical modulator (AOM) that could switch on and off the laser beam in less than a microsecond. Both components were controlled by a computer, which also coordinated the actions of both Scamper and CLSM. Employing the computer of the Scamper, a confocal image could be superimposed by an image mask. During a scanning cycle, the computer activated the AOM such that a pattern was bleached into the sample corresponding exactly to the image mask. The dissipation of the bleach pattern by lateral diffusion was monitored by a series of confocal images generated at non-bleaching conditions (attenuated laser beam).

diffracted upon activation about 70% of the beam power into the first order at a contrast ratio of 2.000/1 with a rise time of switching of ~100 ns. Beyond the AOM, a mirror reflected the first-order-beam into the CLSM, where it was focused onto the illumination pinhole. The Scamper also included an interface to transform TTL signals into appropriate signals for the filter box and the AOM driver. A standard 386/40-computer (PC) with 8 MHz-ISA-data bus controlled filter changer and AOM, and maintained communication to the CLSM workstation via the parallel port. Comprehensive software, referred to as ScampMaster, for control and evaluation of scanning microphotolysis experiments was developed in C and assembler as a Microsoft-Windows application.

A Scamp experiment proceeds as follows. Using the attenuated laser beam (attenuating filters inserted, AOM permanently activated), a prebleach image is generated on the CLSM and transferred to the computer of the Scamper. In the prebleach, image areas to be bleached are selected by creating an image mask. A bleaching scanning cycle is then initiated. At first, the computer of the Scamper removes the attenuating filters from the laser beam. Then, using trigger signals issued by the CLSM workstation at the beginning of each line the computer of the Scamper activates the AOM during scanning such that a pattern is bleached into the sample which corresponds exactly to the image mask. We have observed that the spatial accuracy of photobleaching was about ±2.5 pixels, i.e., equal or better than diffraction limited resolution at most scanning conditions. Typically (scanned area = 31x31 $\mu m^2$, image format = 512x512 pixel), a pixel measures (0.0612 $\mu m)^2$. Also, photobleaching was observed to be sufficiently effective. Using human erythrocyte ghosts loaded with a fluorescein-labeled 70 kDa dextran as test system, a 40-fold, NA 1.3 oil immersion objective lense and a laser power of about 1 mW in the sample we found that the fluorescence of the ghosts was reduced by 12.5% by a single bleaching cycle. Six to eight repetitions were necessary to induce a 50% reduction of fluorescence.

In the present study, Scamp experiments were performed in the following manner. A suitable cell was selected, and the cell surface adhering to the coverslip was brought into focus. A prebleach image was generated, and circular areas were selected for bleaching on the cell surface by means of an image mask. The bleaching scanning cycle was performed in such a manner that the integral intensity of the bleached areas was reduced by approximately 50%. Then a series of (usually) 10 images was recorded at nonbleaching conditions using appropriate time delays.

## Data analysis

The raw data of a single experiment consisted of a stack of $N = 11$ images taken at time points $t_i$, corresponding to ~2.5 MB of image data. The first image was the prebleach recording; the last was an image taken after an extended period of time, when the fluorescence recovery process had been completed. Before data analysis, the images were smoothed with a 3x3 median filter. This removed high frequency noise and corrected for pixels with values exceeding the eight-bit limit. Then the images were scaled to each other to correct for the very small degree of photobleaching occurring during acquisition of the monitor images, i.e., approximately 1% fluorescence reduction per image.

To prepare the images for computation of the radial distribution function of the photobleached fluorophores, they were processed in the following way. To correct for intrinsic inhomogeneities in the fluorescence distribution within the observed cell membrane region, the prebleach image was divided by each monitor image resulting in a series of quotient images. Before this operation, the prebleach image was smoothed with a 15x15 Gauss kernel to prevent an amplification of the image noise by the division. Furthermore, because the division usually resulted in images with intensity values between 0 and 2 (photobleaching ≤50%), the computations were performed using floating point variables that were scaled by a factor of $2^7$ before storing the results as integer value images.

The radial distribution function of the photobleached fluorophores was calculated from the scaled quotient images. All pixels inside a circle of radius $r_0 = 3w$ around the center of the circular bleaching spot were evaluated. The pixel values were radially averaged, resulting in a set of floating point values $g_i'(r)$ for each image $i$. Finally, we computed $g_i(r) = g_i'(r) - c$, where $c$ was the average value of $g_i'(r)$ for large $r$ of images $i = 2$ to 7, where the pixel values were virtually constant over distance to the center and time. This yielded a corrected distribution function that decayed to zero for large $r$.

As discussed in the theory section, we used the distributions $g_i(r)$ directly to determine $D$. For that purpose, each single data set $g_i(r)$ was fitted directly by an expression derived from Eq. 3, i.e.,

$$g_i(r) = Bw \int_0^{r_e} e^{-Dts^2} J_0(sr) J_1(ws)\, ds. \qquad (12)$$

Fitting was performed employing a nonlinear $\chi^2$-minimization routine based on a Levenberg-Marquardt method using $D$ and $B$ as parameters (Press et al., 1992). Here, $B$ is an arbitrary amplitude parameter, a constant value was used in the evaluation of all images belonging to the same stack. It can eventually be used for determination of the distribution immediately after bleaching, $g_{t=0}(r)$, corresponding to $F(0)$ in the conventional analysis. The mobile fraction of fluorophores, determined as described below, was assumed to be constant within the bleached area and taken appropriately into account by the fitting routine. The integration was performed numerically from 0 to $r_e$ employing a Romberg integration scheme. We found this integration to be not trivial; much care had to be taken in choosing the appropriate integration limit, $r_e$, the stepsizes, and the accuracy of the integration process.

From the radial distribution function the sum of the two second central moments $\mu_{2,i}$ was calculated as

$$\mu_{2,i} = \langle r^2 \rangle = \int_0^\infty r^3 g_i(r)\, dr \Big/ \int_0^\infty r g_i(r)\, dr. \qquad (13)$$

$\mu_{2,i}$ was then plotted versus $t_i$, and a straight line was fitted to this data to obtain $D$ times $k$ from its slope according to Eq. 11. Finally, knowing $k$ (see below), $D$ was calculated.

As the last step, the mean intensity within the photobleached area was determined in all images. This yielded a prebleach fluorescence value $F_{ave,pre}$ and values $F_{ave,i}$ for all time points $t_i$. These data were fitted by Eqs. 5 and 6 as described above. Thus, $D$, $F(0)$, and $F(\infty)$ were determined and, using Eq. 7, the mobile fraction $k$ was derived.

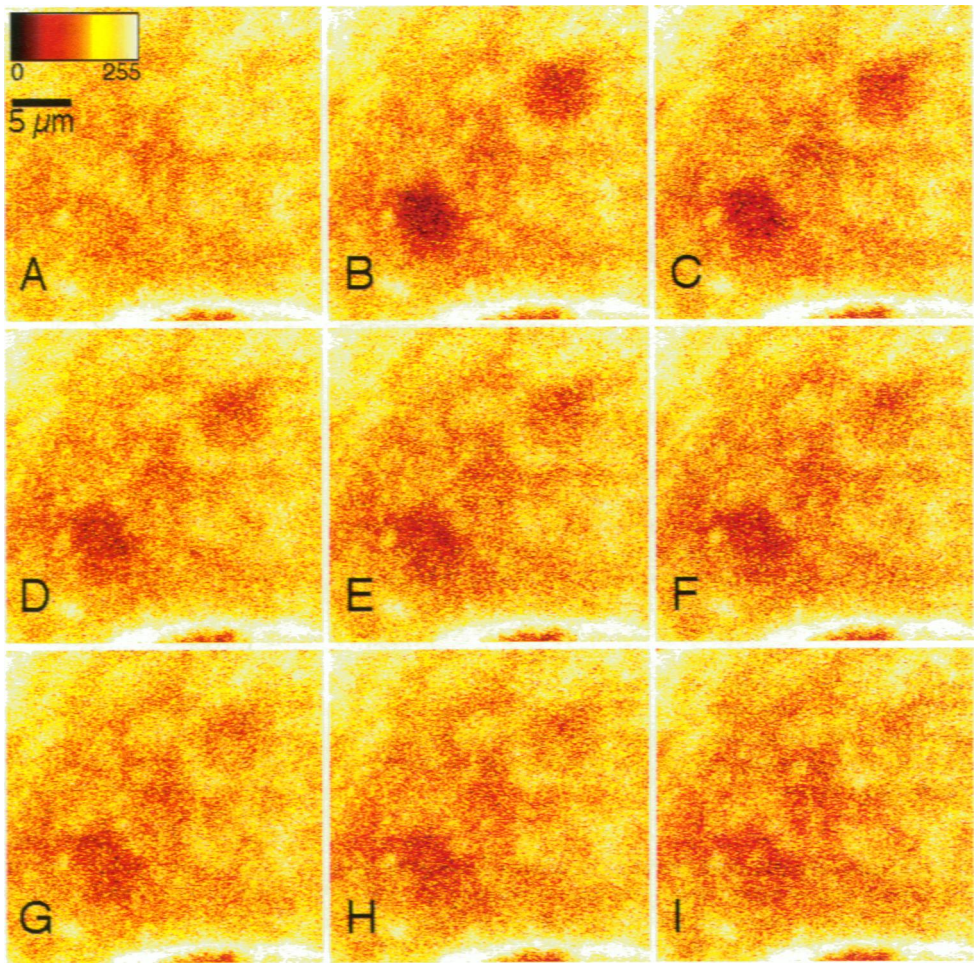


Fig. 2*a*.

FIGURE 2 A Scamp experiment relating to the lateral mobility of plasma membrane lipids. The surface of a 3T3 cell that had been labeled with the fluorescent lipid analog NBD-HPC was imaged by confocal laser scanning microscopy at high resolution (note the scale). Only a part of the cell surface can be observed; the cell border is visible at the lower edge. Images were obtained before (*A*) and at various times after (*B–I*) photobleaching of two circular membrane areas. The dissipation of the bleach pattern by lateral mobility can be recognized. (*a*) Unprocessed images; (*A*) prebleach image; (*B–H*) monitor images taken at times $t_B$ = 3.3 s, $t_C$ = 6.8 s, $t_D$ = 10.3 s, $t_E$ = 14.6 s, $t_F$ = 18.3 s, $t_G$ = 23.7 s, $t_H$ = 30.0 after the bleach scanning, and (*I*) acquired after completion of the fluorescence redistribution ($t_I$ = 80 s). (*b*) Processed images. In *A*, the unprocessed prebleach image (*a*, *A*) was smoothed with a 3x3 median filter and 15x15 Gauss kernel, revealing that the fluorescence of the cell surface was intrinsically inhomogeneous. (*B–I*) Smoothed, scaled, and inverted images were generated by dividing the smoothed prebleach image (*A*) by the respective smoothed monitor images (*a*, *B–I*). The improvement of image quality by smoothing and normalizing is apparent.

Image processing was performed partly by software written by us in C, partly using the program "NIH Image," V 1.52, by Wayne Rasband. All data evaluation, simulating, and fitting programs were written in C.

## RESULTS

The new method, Scamp, was applied to study the lateral mobility of the fluorescent lipid analog NBD-HPC in the plasma membrane of living 3T3 cells. Cells were labeled, and measurements were performed as described above. First, an example for the raw data and their processing will be given. Then three different methods for the evaluation of the data in terms of mobility coefficients will be described.

A representative experiment is shown in Fig. 2. Here, two circular areas with a radius of 3.0 $\mu$m were bleached simultaneously on one cell, demonstrating one of the novel possibilities offered by Scamp. The magnification was chosen such that an area of 31 × 31 $\mu m^2$ was imaged. Therefore, only a central part of the cell can be recognized, a cell boundary being visible at the bottom.

Unprocessed raw images are shown in Fig. 2 *a*. This series consists of a prebleach image (*A*), seven monitoring images taken at various times after bleaching (*B–H*: $t_B$ = 3.3 s, $t_C$ = 6.8 s, $t_D$ = 10.3 s, $t_E$ = 14.6 s, $t_F$ = 18.3 s, $t_G$=23.7 s, $t_H$ = 30.0 s) and a final image, acquired after completion of the fluorescence redistribution ($t_I$ = 80 s). To minimize phobleaching during observation, the power of the laser beam was kept very small. In addition, the number of line scanning averages was set to be only 2. Therefore, the images were quite noisy. Nevertheless, inspection of the prebleach image (Fig. 2 *a*, *A*) clearly reveals that the plasma membrane did not fluoresce homogeneously. Inhomogeneities as observed in Fig. 2 *a* (*A*) were present in all of the images acquired for this study and presumably reflect an inhomogeneity of the plasma membrane itself. Fig. 2 *a* also reveals that fluorescence inhomogeneities were rather stable and persisted in the complete image series.

Smoothed inverted ratio images (Fig. 2 *b*), rather then raw images (Fig. 2 *a*), were used for the further evaluation. The inverted ratio images were generated by division of the smoothed prebleach image (Fig. 2 *b*, *A*) by the respective monitor image. This operation dramatically improved the image quality. Nevertheless, we found it necessary to reduce further the noise before the images could be evaluated in terms of diffusion coefficients. For this purpose several different smoothing approaches were employed and carefully compared to verify that no erroneous data were artificially produced. The final result is shown in Fig. 2 *b* (*B–H*). It should be stressed again that the images were inverted. Thus,

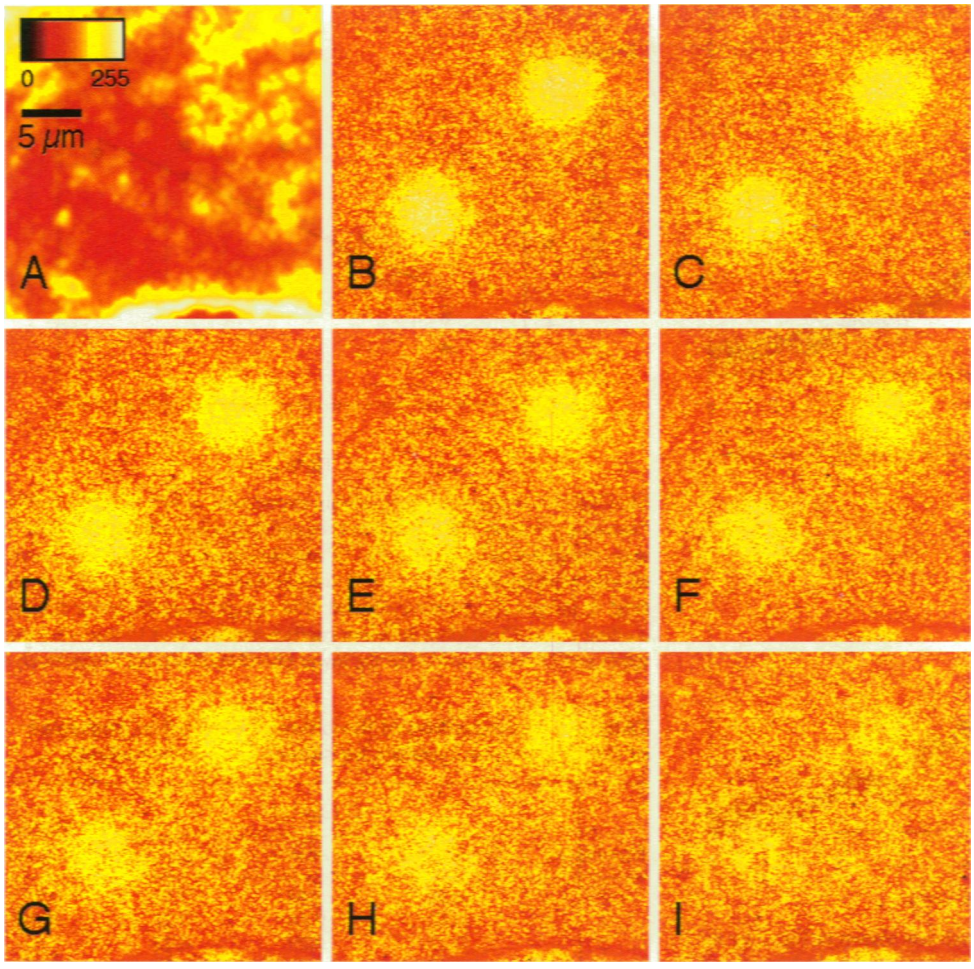


Fig. 2*b*.

large intensities represent high concentrations of bleached rather than nonbleached chromophores.

A first method for evaluating Scamp data in terms of mobility coefficients is illustrated in Fig. 3. For each image of Fig. 2 *b*, the radial distribution function of bleached dye molecules (*open symbols*) was calculated. This was done separately for the two bleached membrane areas to yield two sets of distribution functions for the upper (Fig. 3 *a*) and the lower bleached area (Fig. 3 *b*), respectively. The spreading of bleached chromophores with time can be clearly recognized. The time interval used for data evaluation (30 s) was short enough to warrant that the two distribution would not distort each other. The noisy nature of the distributions near the center of the photobleached area is because only a small number of pixel values contribute to the radial averages of $g_i(r)$ for small values of $r$. To derive the diffusion coefficient, theoretical curves were calculated according to Eq. 12 and fitted by a $\chi^2$-minimization routine to the experimental data (*solid* and *dashed lines*). Thus, each image of the series of Fig. 2 *b* yielded, for both of the bleached areas independently, values for the diffusion coefficient. Averaging these values for the whole image series yielded $D_1 = 0.28 \pm 0.03$ $\mu m^2/s$ for the upper and $D_2 = 0.24 \pm 0.02$ $\mu m^2/s$ for the lower membrane area, respectively.

Fig. 4 illustrates a second method of data evaluation. Here, the variance was calculated according to Eq. 13 for the radial distribution functions shown in Fig. 3. The calculated values were then plotted versus time and fitted by a straight line to yield $D_1 = 0.15 \pm 0.06$ $\mu m^2/s$ (*filled circles, solid line*, upper membrane area) and $D_2 = 0.25 \pm 0.06$ $\mu m^2/s$ (*filled squares, dashed line*, lower membrane area), respectively. These results agree quite well with the outcome of the other evaluation methods (c.f. below and Table 1), despite the fact that they scatter considerably (Fig. 4). The scattering is probably because the third power of the radius appears as a factor in the integral (Eq. 13), thus enhancing image noise.

A third method of data evaluation, simulating the one used in conventional photobleaching experiments, is illustrated in Fig. 5. Here the average intensity was calculated for the two bleached membrane areas of Fig. 2 and plotted versus time. The experimental data were then fitted by Eqs. 5–7. Because the relatively low repetition rate of image acquisition, which was 0.3 $s^{-1}$ in the employed scanning mode, we were not able to determine the fluorescence value right after bleaching, i.e., $F(0)$. Hence, we chose to leave this value as a free parameter in the fitting routine. This yielded $D_1 = 0.19$ $\mu m^2/s$ (*circles*, upper membrane area) and $D_2 = 0.23$ $\mu m^2/s$ (*squares*, lower

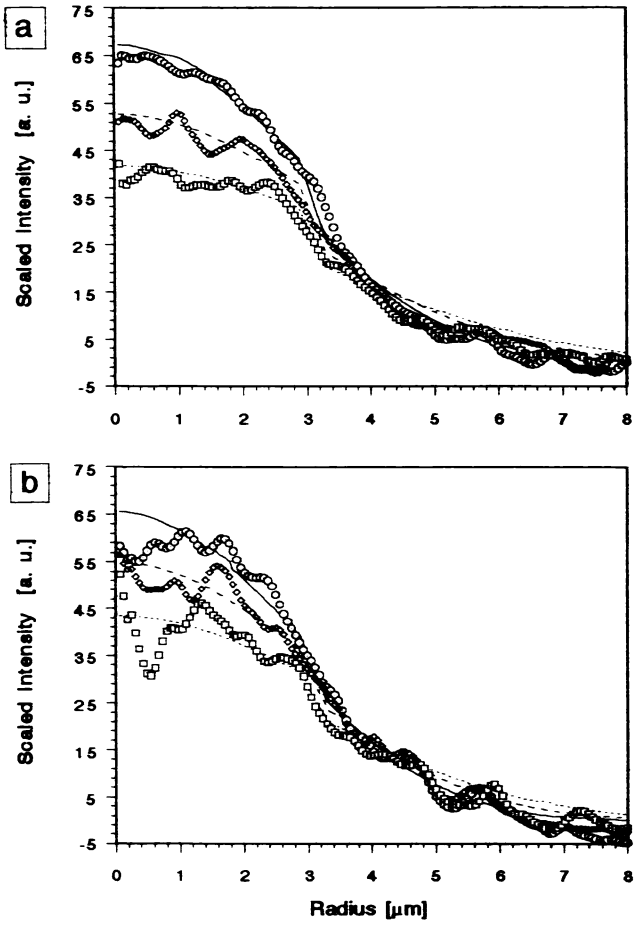


FIGURE 3 Evaluation of the Scamp experiment shown in Fig. 2 by the "distribution" method. The radial distributions (*open symbols*) of photolysed dye molecules around the center of the photobleached areas were derived from Fig. 2 and fitted by theoretical curves (——) according to Eq. 14. The noise for small radius values is caused by the low number of pixels averaged there. (*a*) Upper photobleached area. Radial distribution at $t$ = 3.3 s (○), 10.3 s (◇), and 18.3 s (□) after photobleaching, respectively. (*b*)Lower photobleached area. Radial distribution at $t$ = 6.8 s (○), 10.3 s (◇), and 18.3 s (◇) after photobleaching, respectively.

membrane area), respectively. As above, these values agree quite well with the outcome of the other evaluation methods (cf. Table 1).

The results of 15 Scamp experiments, conducted in the manner illustrated above, are listed in Table 1. Each stack of images was evaluated by the three different methods described. The results are listed for each method of evaluation, together with the corresponding mean values and SDs. The results obtained by fitting the theoretical curve directly to the radial distribution function (column "distributions") are averages of the respective images series. Together, the results agree with each other within the error range. For comparison, we have also used a conventional photobleaching instrument (see Materials and Methods) to measure lipid mobility in the same cells. This yielded $D = 0.26 \pm 0.07$ $\mu m^2/s$, thus confirming the results obtained by Scamp.

## DISCUSSION

This paper describes the application of a new photobleaching method, Scamp, to the analysis of membrane lipid mobility.

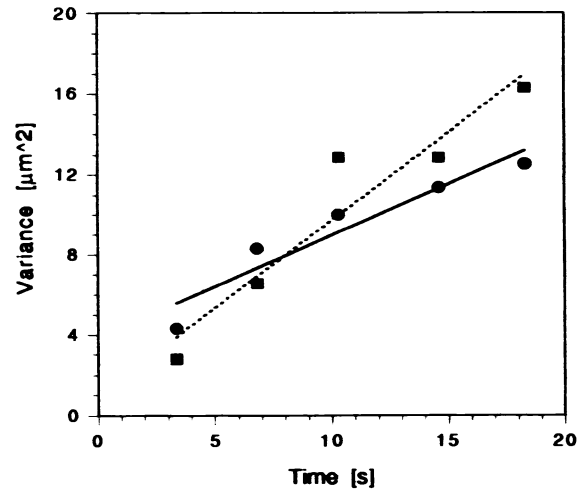


FIGURE 4 Evaluation of the Scamp experiment shown in Fig. 2 by the "variance" method. The variances of the radial distributions shown in Fig. 3 were calculated according to Eq. 13 and plotted versus time. Only distributions from images taken at times smaller than 20 s after photobleaching (Fig. 2, images *B–F*) were evaluated. The straight lines are linear fits according to Eq. 12 yielding diffusion coefficients of $D = 0.15$ $\mu m^2/s$ for the upper and $D = 0.25$ $\mu m^2/s$ for the lower photobleached area, respectively.

**TABLE 1 Comparison of the different evaluation strategies of diffusion measurements by scanning microphotolysis**

| Experiment | $D$ ($\mu m^2/s$)* | | | Mobile fraction |
|---|---|---|---|---|
| | Distributions‡ | Variance | Integral spot | |
| 1 | 0.34 | 0.40 | 0.32 | 0.85 |
| 2 | 0.12 | 0.18 | 0.22 | 0.70 |
| 3 | 0.27 | 0.29 | 0.28 | 0.82 |
| 4 | 0.45 | 0.19 | 0.20 | 0.63 |
| 5 | 0.24 | 0.12 | 0.14 | 1.02 |
| 6 | 0.30 | 0.13 | 0.29 | 0.81 |
| 7 | 0.37 | 0.21 | 0.22 | 0.75 |
| 8 | 0.40 | 0.30 | 0.27 | 0.92 |
| 9 | 0.40 | 0.40 | 0.26 | 0.85 |
| 10 | 0.28 | 0.15 | 0.19 | 0.86 |
| 11 | 0.24 | 0.25 | 0.23 | 0.89 |
| 12 | 0.39 | 0.19 | 0.27 | 0.78 |
| 13 | 0.44 | 0.17 | 0.27 | 0.94 |
| 14 | 0.23 | 0.17 | 0.49 | 0.83 |
| 15 | 0.41 | 0.13 | 0.22 | 0.92 |
| Mean§ | 0.33 | 0.22 | 0.26 | 0.84 |
| SD | 0.09 | 0.09 | 0.08 | 0.10 |

* Diffusion coefficients were determined by each of the three evaluation methods discussed in the Theory section.

‡ Values are weighted averages of the results attained by fits to the fluorescence distributions determined from all but the last image.

§ Conventional photobleaching measurements, which were performed on the very same samples, yielded $D = 0.26 \pm 0.07$ $\mu m^2/s$ ($n$ = 17).

We equipped a CLSM with a more powerful laser and a novel device, the Scamper. This permitted us to switch the laser beam on and off during the scanning process according to a freely definable image mask. Thus, almost any pattern desired could be bleached into the fluorescence of the sample. In the present study, we bleached circular areas onto the surface of single living 3T3 cells that had been labeled with the fluorescent lipid analog NBD-HPC. Subsequently we observed the redistribution of fluorescent probe molecules at the spatial resolution of the CLSM using a low intensity laser beam for fluorescence excitation. The images obtained in this

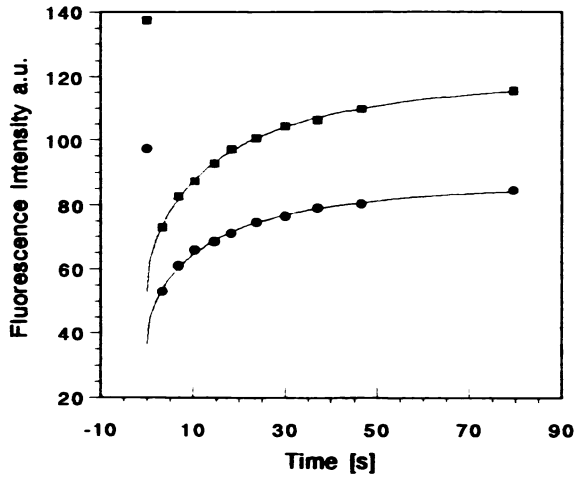


FIGURE 5 Evaluation of the Scamp experiment shown in Fig. 2 by the "integral spot" method, which mimics the evaluation of conventional photobleaching measurements. The intensities of the bleached areas were integrated (*filled symbols*) and plotted versus time. The experimental data were fitted by Eqs. 5–7, yielding values for the diffusion coefficient $D$ of 0.19 and 0.23 $\mu m^2/s$, and for the mobile fraction of 0.86 and 0.89 for the upper and lower photobleached area, respectively.

manner were processed in a particular way and then used to compute the radial distribution functions of photolysed molecules. Having these distribution functions at our disposal, we introduced and tested two new concepts for the determination of lateral mobility coefficients in radially symmetrical geometries and compared these approaches with a third one mimicking data evaluation in conventional photobleaching measurements.

In the "distribution method" we derived the diffusion coefficient by directly fitting an appropriate theoretical function to the experimentally determined distribution function. This could be done for each individual image monitoring the redistribution process. Noteworthy, this evaluation method made use of the full information contents of the images. At present, we determined the mobile fraction by a different, quasi-conventional method and used that value in the fitting process. However, in future studies the theoretical model could easily be extended to include two, or more, mobile fractions. In the "variance method" we considered theoretical aspects of the diffusion process and found that the variance of the distribution function is linearly related to the diffusion coefficient, the mobile fraction, and time. Thus, a plot of the variance versus time can be used to derive the diffusion coefficient in a straightforward manner. The ease of this analysis seemed very tempting to us. It is somehow comparable with the method of Jain et al. (1990), who used the linear time dependence of the radius of a Gaussian spot for determination of $D$. In the "integral method" the average intensity of the photobleached area was calculated as a function of time. This was evaluated in terms of diffusion coefficients and mobile fractions using the equations derived by Axelrod et al. (1976) and Soumpasis (1983) for conventional photobleaching studies.

Altogether we found that the mobility coefficients determined by the three methods were the same within experimental accuracy: $D = 0.33 \pm 0.09$ $\mu m^2/s$ (distribution method), $0.22 \pm 0.09$ $\mu m^2/s$ (variance method), and $0.26 \pm 0.08$ $\mu m^2/s$ (integral method), respectively. These values compared favorably with the one determined by us using a conventional photobleaching apparatus, $D = 0.26 \pm 0.07$ $\mu m^2/s$. The values are also consistent with diffusion coefficients reported in the literature for comparable experimental systems, namely $D = 0.3 \pm 0.1$ $\mu m^2/s$ (Kok et al., 1990; Edidin and Stroynowski, 1991; Yechiel and Edidin, 1987).

The application of our method is currently mainly restricted by two conditions: (i) The bleaching time $T$ has to be small as compared with the characteristic transport time, and (ii) virtually all of the bleached molecules have to be contained in that membrane area considered in the evaluation procedure, even at the latest observation time. The first condition presently restricts the range of diffusion coefficients that can correctly be determined to approximately $D \leq 1.0$ $\mu m^2/s$. This range can be increased, however, by enhancing the frequency of image acquisition and reducing the bleached area. The second condition applies only to the variance method, but neither to the distribution nor the integral method. Therefore, using the variance method only images acquired at times $\leq 30$ s were included into the evaluation procedure.

The integral method, mimicking conventional photobleaching measurements, yielded very smooth data that could be excellently fitted (Fig. 5). This is not surprising, because this method averages over a comparatively large cell surface area. Although this averaging yields a good signal-to-noise ratio, it might cover up essential information. This is different if looking at local fluorescence intensities as in Fig. 3. Here, the data are much more noisy and the fit is worse. This may be caused in part by the smaller signal-to-noise ratio. It is also possible, however, that this reflects some fundamental properties of biological membranes. Lateral transport on the cell surface might considerably deviate from simple diffusion in homogeneous media. Our data already suggest that, e.g., the assumption that mobile and immobile fractions are constant quantities, equal at all locations of a cell's plasma membrane, is probably just a crude approximation. In fact, experimental data from different origins (Saxton, 1993; Edidin, 1992; Ishihara and Jacobson, 1993; Webb, 1994) seem to increasingly support the idea that biological membranes are more intricate structures on a nanometer scale than considered previously.

Finally, the spatial and temporal resolution of the method presented in this paper can be compared with that of already existing techniques such as conventional photobleaching, video-assisted photobleaching, and confocal line scanning after photobleaching. In the focal plane, the spatial resolution of all of these methods is similar, amounting to approximately $\geq 0.25$ $\mu m$. Theoretically, confocal imaging improves the lateral resolution by a factor of 1.4. In the direction of the optical axis, however, large differences between the mentioned methods do exist. Conventional photobleaching methods have an axial resolution of approximately 1–2 $\mu m$

(e.g., Scholz et al., 1985), whereas in video-assisted photobleaching, the axial resolution is almost completely lost because the total field of view is illuminated and imaged. In photobleaching methods employing confocal imaging, on the other hand, the axial resolution can be as small as 0.4 $\mu$m (Engelhardt and Knebel, 1993). The time resolution of photobleaching methods is principally limited by the time resolution of the fluorescence measurement. This is $\leq$10 ms in conventional and 33–40 ms in video-assisted photobleaching techniques. In contrast, the time resolution of Scamp, at least in the version described in this paper, is only 250 ms because the maximum frame frequency of the CLSM was 4/s. However, this is not a principal, but a purely technical, limit. More recent commercial CLSMs, for instance, exhibit frame frequencies of up to 30/s, thus matching those of video methods. In photobleaching methods employing confocal line scanning, the time resolution can be much higher because the times required for scanning a single line, with most commercial CLSMs, amount only to $\sim$1 ms.

In summary, we presented the first application of a new scanning photobleaching method to the lateral mobility of membrane lipids. The method permits one to study molecular transport at the resolution of confocal imaging. It is hoped that these new possibility will help to better characterize dynamic properties of biological membranes.

We should like to thank Dr. L. Pratsch for participating in the initial phases of the project.

Support by the Deutsche Forschungsgemeinschaft (grant Pe 138/15–1) is gratefully acknowledged.

## REFERENCES

Axelrod, D., D. E. Koppel, J. Schlessinger, E. Elson, and W. W. Webb. 1976. Mobility measurement by analysis of fluorescence photobleaching recovery kinetics. *Biophys. J.* 16:1055–1069.

Blonk, J. C. G., A. Don, H. Van Aalst, and J. J. Birmingham. 1993. Fluorescence photobleaching recovery in the confocal scanning light microscope. *J. Microsc.* 169:363–374.

Cardullo, R. A., R. M Mungovan, and D. E. Wolf. 1991. Imaging membrane organization and dynamics. *In* Imaging Membrane Organization and Dynamics. T. G. Dewey, editor. Plenum Press, New York.

Cooper, M. S., A. H. Cornell-Bell, A. Chernjavsky, J. W. Dani, and S. J. Smith. 1990. Tubulovesicular processes emerge from trans-golgi cisternae, extend along microtubules, and interlink adjacent trans-golgi elements into a reticulum. *Cell.* 61:135–145.

Crank, J. 1975. The Mathematics of Diffusion. Clarendon Press, Oxford.

Edidin, M. 1992. Patches, posts and fences: proteins and plasma membrane domains. *Trends Cell Biol.* 2:376–380.

Edidin, M., and I. Stroynowski. 1991. Differences between the lateral organization of conventional and inositol phospholipid-anchored membrane proteins. A further definition of micrometer scale membrane domains. *J. Cell Biol.* 112:1143–1150.

Edidin, M., and Y. Zagyansky. 1976. Lateral diffusion of concanavalin A receptors in the plasma membrane of mouse fibroblasts. *Biochim. Biophys. Acta.* 433:209–214.

Engelhardt, J., and W. Knebel. 1993. Konfokale Laser-Scanning-Mikroskopie. *Physik in unserer Zeit* 24:70–78.

Ishihara, A., and K. Jacobson. 1993. A closer look at how membrane proteins move. *Biophys. J.* 65:1754–1755.

Jacobson, K., Z. Derzko, E.-S. Wu, Y. Hou, and G. Poste. 1976. Measurement of the lateral mobility of cell surface components in single, living cells by fluorescence recovery after photobleaching. *J. Supramol. Struct.* 5:565–576.

Jacobson, K., R. Simson, B. Yang, and G. Lee. 1994. Single particle tracking of cell surface components using nanovid microscopy. *Biophys. J.* 66:18*a*. (Abstr.)

Jain, R. K., R. J. Stock, S. R. Chary, and M. Rueter. 1990. Convection and diffusion measurements using fluorescence recovery after photobleaching and video image analysis: in vitro calibration and assessment. *Microvasc. Res.* 39:77–93.

Kapitza, H. G., G. McGregor, and K. A. Jacobson. 1985. Direct measurement of lateral transport in membranes by using time-resolved spatial photometry. *Proc. Natl. Acad. Sci. USA.* 82:4122–4126.

Kok, J. W., M. ter Brest, G. Scherphof, and D. Hoekstra. 1990. A non-exchangeable fluorescent phospholipid analog as a membrane traffic marker of the endocytic pathway. *J. Cell Biol.* 53:173–184.

Koppel, D. E. 1979. Fluorescence redistribution after photobleaching. A new multipoint analysis of membrane translational dynamics. *Biophys. J.* 28:281–292.

Kubitscheck, U., P. Wedekind, and R. Peters. 1994. Scanning microphotolysis: a new photobleaching technique based on fast intensity modulation and confocal imaging. Confocal and Near-field microscopy. April 25–28, Munich, Germany. Abstract.

Kusumi, A., Y. Sako, and M. Yamamoto. 1993. Confined lateral diffusion of membrane receptors as studied by single particle tracking (nanovid microscopy). Effects of calcium-induced differentiation in cultured epithelial cells. *Biophys. J.* 65:2021–2040.

Peters, R., J. Peters, K. H. Tews, and W. Bähr. 1974. A microfluorimetric study of translational diffusion in erythrocyte membranes. *Biochim. Biophys. Acta.* 367:282–294.

Peters, R., and M. Scholz. 1991. Fluorescence photobleaching techniques. *In* New Techniques of Optical Microscopy and Microspectroscopy. R. J. Cherry, editor. Macmillan, New York. 199–228.

Petersen, N. O., S. Felder, and E. L. Elson. 1986. Measurement of lateral diffusion by fluorescence photobleaching recovery. *In* Handbook of Experimental Immunology. Vol. 1. Immunochemistry. D. M. Weir, editor. Blackwell Scientific Publications, Oxford. 24:1–24.23.

Press, W. H., S. A. Teukolsky, W. T. Vetterling, and B. P. Flannery. 1992. Numerical Recipes in C. Cambridge University Press, Cambridge.

Saxton, M. J. 1993. Lateral diffusion in an archipelago. *Biophys. J.* 64: 1766–1780.

Scholz, M., H. Sauer, H. P. Rihs, and R. Peters. 1988. Laser scanning microscopy to study molecular transport in single cells. *SPIE.* 1028: 160–166.

Scholz, M., K. Schulten, K., and R. Peters. 1985. Single-cell flux measurement by continuous fluorescence microphotolysis. *Eur. Biophys. J.* 13:37–44.

Soumpasis, D. M. 1983. Theoretical analysis of fluorescence photobleaching recovery experiments. *Biophys. J.* 41:95–97.

Thomas, J., and W. W. Webb. 1990. Fluorescence photobleaching recovery: a probe of membrane dynamics. *In* Noninvasive Techniques in Cell Biology. J. Thomas and W. W. Webb, editors. Wiley-Liss, New York. 129–152.

Tsay, T.-T., and K. A. Jacobson. 1991. Spatial fourier analysis of video photobleaching measurements. *Biophys. J.* 60:360–368.

Tschödrich-Rotter, M. 1994. Fluoreszenz-Mikrophotolyse: Aufbau einer Apparatur für die Fluoreszenz-Mikrophotolyse und Mobilitätsmessungen am Protein P4 in Zellkernen. Ph.D. thesis. Westfälische Wilhelms-Universität, Münster, Germany.

Webb, W. W. 1994. Fractile time transport in the cell surface. *Biophys. J.* 66:18*a*. (Abstr.)

Wedekind, P., U. Kubitscheck, and R. Peters. 1994. Scanning microphotolysis: a new photobleaching technique based on fast intensity modulation of a scanned laser beam and confocal imaging. *J. Microsc.* In press.

Yechiel, E., and M. Edidin. 1987. Micrometer-scale domains in fibroblast plasma membranes. *J. Cell Biol.* 105:755–760.